VOL.6 NO.2 FEBRUARY 2007
www.nature.com/naturematerials

nature materials

Woven scaffolds to build on

NANOCRYSTAL SUPERLATTICES
Far better than the average

POROUS FRAMEWORKS
Flexible and tunable

PHASE-CHANGE MATERIALS
A manual for improvement

A biomimetic three-dimensional woven composite scaffold for functional tissue engineering of cartilage

FRANKLIN T. MOUTOS[1,2], LISA E. FREED[3] AND FARSHID GUILAK[1,2,4]*

[1]Department of Surgery, 375 MSRB, Box 3093, Duke University Medical Center, Durham, North Carolina 27710, USA
[2]Department of Biomedical Engineering, 375 MSRB, Box 3093, Duke University Medical Center, Durham, North Carolina 27710, USA
[3]Harvard-MIT Division of Health Sciences & Technology, Massachusetts Institute of Technology, 77 Massachusetts Avenue, Building E25-330, Cambridge, Massachusetts 02139, USA
[4]Department of Mechanical Engineering & Materials Science, 375 MSRB, Box 3093, Duke University Medical Center, Durham, North Carolina 27710, USA
*e-mail: guilak@duke.edu

Published online: 21 January 2007; doi:10.1038/nmat1822

Tissue engineering seeks to repair or regenerate tissues through combinations of implanted cells, biomaterial scaffolds and biologically active molecules. The rapid restoration of tissue biomechanical function remains an important challenge, emphasizing the need to replicate structural and mechanical properties using novel scaffold designs. Here we present a microscale 3D weaving technique to generate anisotropic 3D woven structures as the basis for novel composite scaffolds that are consolidated with a chondrocyte–hydrogel mixture into cartilage tissue constructs. Composite scaffolds show mechanical properties of the same order of magnitude as values for native articular cartilage, as measured by compressive, tensile and shear testing. Moreover, our findings showed that porous composite scaffolds could be engineered with initial properties that reproduce the anisotropy, viscoelasticity and tension–compression nonlinearity of native articular cartilage. Such scaffolds uniquely combine the potential for load-bearing immediately after implantation *in vivo* with biological support for cell-based tissue regeneration without requiring cultivation *in vitro*.

Articular cartilage, the smooth wear-resistant tissue that lines the ends of bones in diarthrodial joints, serves to support and distribute applied loads[1] and functions biomechanically as a multiphasic fibre-reinforced material with anisotropic, inhomogeneous, nonlinear and viscoelastic properties[2–4]. These complex mechanical properties provide the essential mechanism for pressurization of the interstitial fluid of the tissue under stress, allowing for the crucial load-support and low-friction properties of the tissue. Therefore, the engineered repair of cartilaginous tissues has remained particularly challenging from a biomechanical standpoint[5]. The goal of this study was to create a novel scaffold for cartilage tissue engineering that qualitatively and quantitatively mimicked the mechanical properties and behaviours of articular cartilage and was made of biocompatible materials previously shown to be conducive to chondrogenesis (for example polyglycolic acid[6], agarose[7] or polyglycolic acid and fibrin[8]). In contrast to previously used cartilage tissue engineering scaffolds such as non-woven textiles[6,9–13], hydrogels[7,14–18] or a combination of the two[8,19], which typically showed isotropic biomechanical properties[20], we sought to develop a scaffold with multidirectional biomechanical behaviour mimicking the anisotropy of native cartilage. Furthermore, in contrast to previously used scaffolds that typically show stiffness and strength that are several orders of magnitude lower than native cartilage[11,16,21], we sought to develop a scaffold with properties similar to those of native cartilage *a priori*, potentially avoiding a protracted *in vitro* culture process (for example from 4–8 weeks[6,11,12,16] to 7 months[9]).

We developed a novel microscale weaving technology to generate three-dimensional (3D) structures with fibres oriented in three orthogonal directions using a custom-built weaving loom that was specifically constructed to produce orthotropic, porous textile structures with prescribed mechanical properties starting from small diameter, biodegradable yarns. In comparison to standard weaving methods, this process eliminates fibre crimp and forms a true 3D structure by interlocking multiple layers of two perpendicularly oriented sets of in-plane fibres (x- or warp direction, and y- or weft direction) with a third set of fibres that pass through the thickness (z-direction) of the fabric structure (Fig. 1)[22]. Additional advantages include the specification of fibre spacing and volume fraction in each axis, and the selection of each individual fibre in the construct to allow for controlled anisotropy and depth-dependent properties. The 3D porous structures were produced using 104-μm-diameter continuous multifilament polyglycolic acid yarn (Biomedical Structures LLC, Slatersville, Rhode Island). The yarn was woven into two different 3D structures containing a total of 11 in-plane fibre layers; five layers were oriented in the warp (0° or lengthwise in the loom) direction and six layers were oriented in the weft (90° to the lengthwise fibres) direction. The first, 'small-pore', structure contained 24 yarns per centimetre in each of the five warp layers, 20 yarns per centimetre in each of the six weft layers and 24 yarns per centimetre in the Z-direction. Its interconnected internal pores had dimensions of 390 μm × 320 μm × 104 μm, yielding a total void volume of ~70%. The second, 'large-pore', structure was similar to the first except

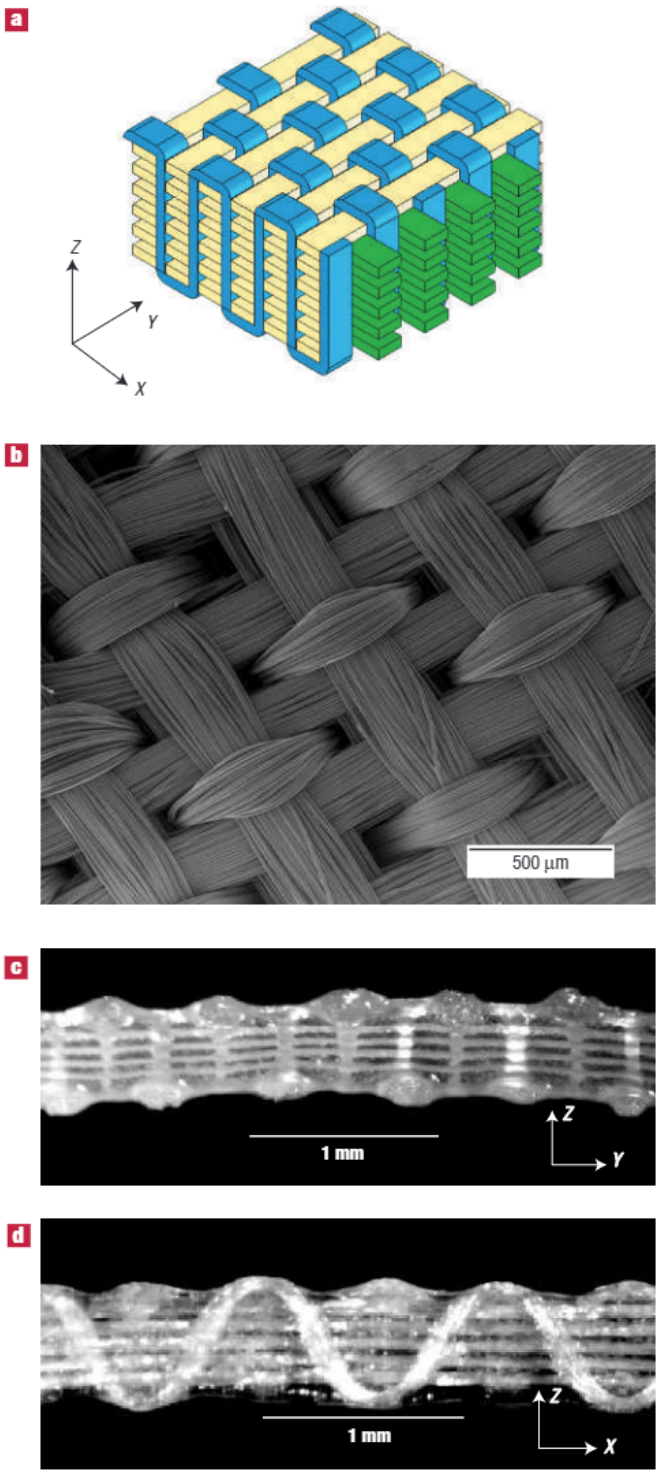

Figure 1 Fibre architecture of a 3D orthogonally woven structure. 3D structures were woven by interlocking multiple layers of two perpendicularly oriented sets of in-plane fibres (*x*- or warp direction, and *y*- or weft direction) with a third set of fibres in the *z*-direction. **a**, Schematic diagram; **b**, surface view of the *X*–*Y* plane (scanning electron microscope); **c**, cross-sectional view of the *Y*–*Z* plane; **d**, cross-sectional view of the *X*–*Z* plane.

that it contained only 15 yarns per centimetre in each of the six weft layers, and had pore dimensions of 450 µm × 320 µm × 104 µm, with a total void volume of ~74%.

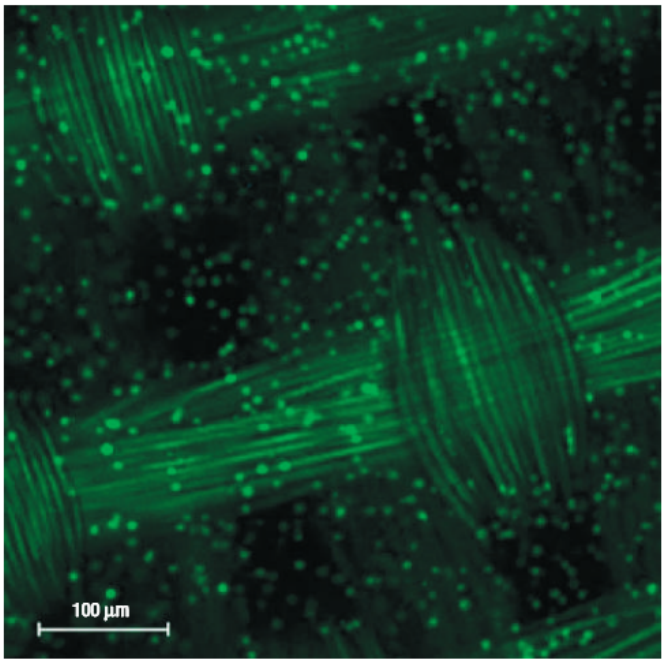

Figure 2 Fluorescent image of a freshly seeded construct. Porcine articular chondrocytes in a fibre-reinforced 2% agarose (small pore scaffold) show a spatially uniform initial distribution of cells with rounded morphology (fluorescent labelling with calcein-AM).

We used the 3D porous structures, once woven, to generate fibre-reinforced composite materials conducive to cell growth by consolidation with a biocompatible hydrogel[8,19,20,23]. In particular, we generated composite scaffolds by vacuum-assisted infusion of a biocompatible hydrogel or cell–hydrogel mixture. We evaluated typically used hydrogels, agarose (2% or 3% w/v) and fibrin (100–130 mg ml^{-1}, Tisseel, Baxter Biosurgery, Westlake Village, California). Using this technique, we readily seeded scaffolds with a spatially uniform distribution of cells (Fig. 2) that maintained the rounded morphology important in promoting a chondrocytic phenotype[14,16,18,24,25]. For this study, however, we carried out tests on composite scaffolds without cells to determine their initial biomechanical properties *a priori*. The 3D woven composite scaffolds showed significant anisotropic, nonlinear and viscoelastic properties that were similar to those of native articular cartilage. With the exception of tensile moduli, which were higher for composites than native cartilage, all evaluated composite properties were of the same order of magnitude as the native tissue (Table 1).

As expected, composite mechanical properties depended significantly on the presence of 3D fibre reinforcement and the size of the pores (Fig. 3). Fibre-reinforced, 2% agarose (small-pore-scaffold) composites showed fourfold higher aggregate moduli and 15-fold higher Young's moduli than unreinforced agarose (Fig. 3a, $p < 0.005$). Scaffolds woven with small pores showed significantly higher aggregate moduli than those woven with large pores in confined compression (Fig. 3b, $p < 0.005$). The mean values of aggregate modulus for the small- and large-pore scaffolds were 199 ± 18 kPa and 138 ± 11 kPa, respectively (mean ± SEM). Similar trends were seen in unconfined compression, where mean values for Young's modulus were 77 ± 24 kPa for small-pore scaffolds and 68 ± 18 kPa for large-pore scaffolds (Fig. 3b). However, for a given woven structure the type of hydrogel (2% agarose, 3% agarose or 100–130 mg ml^{-1} fibrin) did not have any significant effect on the compressive properties of the composite (Fig. 3b). The

Table 1 Biomechanical properties of composite scaffolds are compared with native articular cartilage. Ranges given for the composite scaffolds include all experimental groups (that is two types of woven structure and three types of hydrogel).

	Composite scaffold	Articular cartilage
Tensile properties		
Ultimate tensile stress	75–85 MPa	15–35 MPa (refs 33,39)
Ultimate tensile strain	22–27%	10–40% (refs 33,39)
Tensile modulus (10% ε)	325–400 MPa	5–25.5 MPa (refs 32,35,40)
Poisson's ratio	0.073–0.076	0.9–2.2 (ref. 41)
Equilibrium relaxation modulus	150–200 MPa	6.5–45 MPa (refs 42,43)
Compressive properties		
Aggregate modulus	0.14–0.2 MPa	0.1–2.0 MPa (ref. 44)
Hydraulic permeability	$0.4–1.0 \times 10^{-15}$ m^4 N^{-1} s^{-1}	$0.5–5.0 \times 10^{-15}$ m^4 N^{-1} s^{-1} (refs 45,46)
Young's modulus	0.005–0.1 MPa	0.4–0.8 MPa (refs 47,48)
Shear properties		
Equilibrium shear modulus	0.03–0.05 MPa	0.05–0.25 MPa (refs 38,49)
Complex shear modulus	0.09–0.11 MPa	0.2–2.0 MPa (ref. 38)
Loss angle	~35°	~10° (ref. 38)

apparent hydraulic permeability showed no significant dependence on the type of woven structure or the type of hydrogel (Fig. 3c). Likewise, no significant differences in shear moduli were observed with respect to the type of woven structure or hydrogel (Fig. 3d).

Importantly, composite mechanical properties mimicked the anisotropy, viscoelasticity and tension–compression nonlinearity of native articular cartilage (Table 1, Figs 3 and 4). The ability of articular cartilage to withstand extremely high mechanical

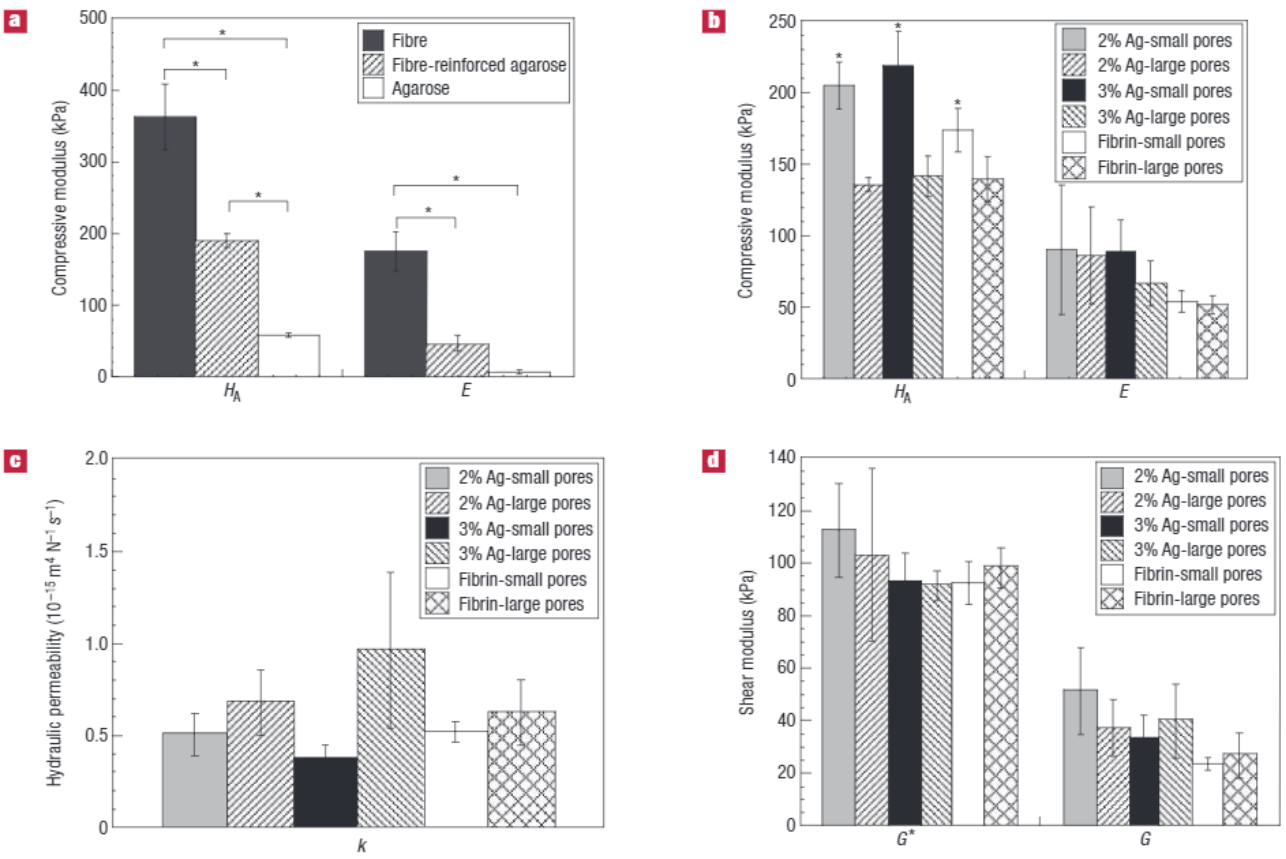

Figure 3 Effects of fibre reinforcement on compressive and shear mechanical properties. a,**b**, Aggregate modulus (H_A) and Young's modulus (E) as determined by confined and unconfined compression, respectively. **a**, Fibre-reinforced 2% agarose (small-pore scaffold) had significantly higher H_A and E than unreinforced 2% agarose. Data presented are mean ± SEM. $^*p < 0.05$. **b**, Scaffolds woven with small pores showed significantly higher H_A than large-pore scaffolds. Data presented are mean ± SEM. $^*p < 0.005$. **c**, Hydraulic permeability (k) as determined by curve-fitting creep tests using a nonlinear numerical least-squares regression procedure. **d**, Complex shear modulus (G^*) and equilibrium shear modulus (G) determined by dynamic testing at angular frequency $\omega = 10$ rad s^{-1} and an amplitude $\gamma_0 = 0.05$ and stress-relaxation shear testing, respectively.

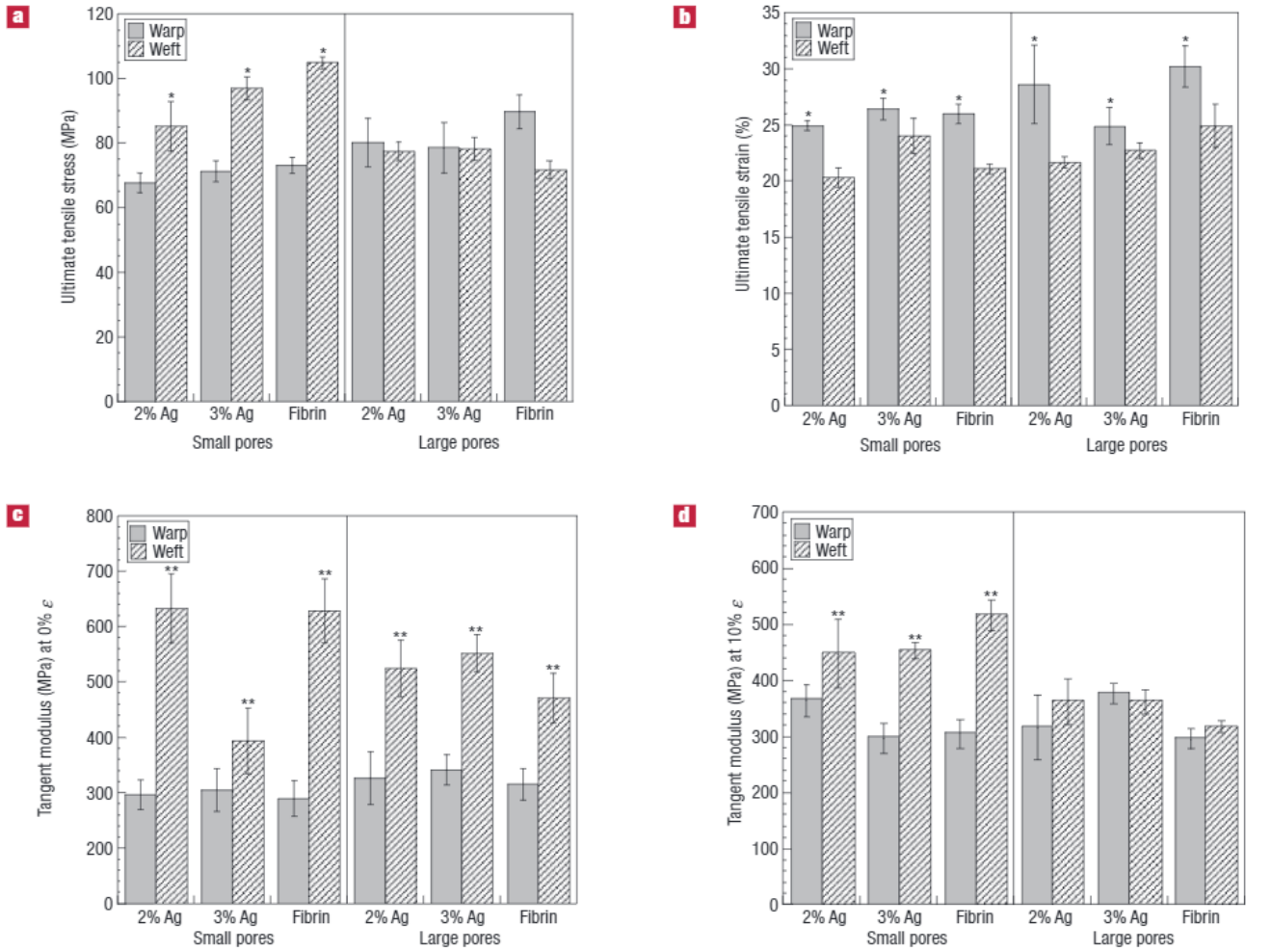

Figure 4 Effects of fibre reinforcement on tensile properties. Properties were measured in the warp (X) and weft (Y) directions (filled and hatched symbols, respectively). **a**, Small-pore scaffolds had significantly higher ultimate tensile stresses in the weft than in the warp direction. Data presented are mean ± SEM. $^{*}p < 0.05$. **b**, Both scaffold structures had significantly higher ultimate tensile strains in the warp than in the weft direction. Data presented are mean ± SEM. $^{*}p < 0.05$. **c**, Tangent moduli at 0% strain in the warp and weft directions. Data presented are mean ± SEM. $^{**}p < 0.0001$. **d**, Tangent moduli at 10% strain in the warp and weft directions. Data presented are mean ± SEM. $^{**}p < 0.0001$.

stresses has been attributed to the complex ultrastructure and mechanical properties of the tissue. In particular, tension–compression nonlinearity, which accounts for approximately two orders of magnitude difference between the tensile and compressive moduli of native cartilage[3,26,27], is believed to play an important role in its load-bearing capacity by enhancing fluid pressurization under compression[28,29]. In this respect, the design of the 3D fibre scaffold mimics the behaviour of cartilage as a fibre-reinforced composite, albeit at a larger scale (microscale instead of nanoscale fibres)[30]. The extent of fluid load support is highly dependent on this tension–compression nonlinearity[3], which theoretically provides for 98% of the load to be supported by fluid pressure in native cartilage. In our scaffold, this value approaches 100% owing to the higher-than-normal tensile modulus. Resistance to compressive loading, however, seemed to arise predominantly from inter- and intra-fibre friction among the constituent multifilament yarns within the weave. Even though the hydrogel component seemed to be primarily responsible for the observed viscoelastic creep behaviour, changes in hydrogel composition did not contribute significantly to the compressive properties of the composite scaffolds (Fig. 3b), consistent with previous reports[7,16]. The apparent hydraulic permeability of the structure, as measured by confined compression creep, was similar to that of native cartilage ($\sim 10^{-15}$ m^4 N^{-1} s^{-1}), but significantly lower than that measured directly for agarose[31], reflecting additional biomimetic properties of the composite scaffolds. Additional tests examining the level of fluid pressurization would provide more direct evidence for the role of the fluid phase in load support[29].

Significant anisotropy was observed in the ultimate tensile stress, ultimate tensile strain and tensile moduli at 0% and 10% strain (Fig. 4a–d, respectively). Skeletally mature articular cartilage shows significant anisotropy in tension relative to the preferred orientation of collagen fibres in the surface zone, or local 'split-line' direction[4,32–34]. For example, the tensile failure stress of native cartilage parallel to the split-line direction has been shown to be twice as high as that perpendicular to the split-line direction[33]. The small-pore scaffolds developed in this study were designed to have similar in-plane directional dependences of tensile mechanical properties. In particular, anisotropy of the ultimate tensile strength and tensile modulus was achieved in the small-pore scaffolds (Fig. 4a,c,d) by designing a biased woven structure that contained a higher fibre volume fraction in the weft direction

than in the warp direction (Fig. 1a). This anisotropy, however, was not present in the large-pore scaffolds, which were woven with more balanced warp–weft fibre volume fractions. Alternatively, controlled anisotropy independent of the pore size or fibre packing density could be achieved by using fibres with different sizes or chemical compositions in any of the orthogonal directions. Small-pore scaffolds showed ~35% higher ultimate tensile stress when tested in the weft direction than in the warp direction (Fig. 4a, $p < 0.05$), a finding that did not apply to large-pore scaffolds. Tensile moduli calculated at 0% strain (E_0) for all scaffolds were significantly higher when tested in the weft direction than in the warp direction (Fig. 4c, $p < 0.0001$). However, only small-pore scaffolds showed significantly higher tensile moduli at 10% strain (E) when tested in the weft direction as opposed to the warp direction (Fig. 4d, $p < 0.0001$). Values of E_0 were up to ~250% greater in the weft direction as compared to the warp direction, whereas values for E were only ~25% higher (Fig. 4c versus d). On average, tensile moduli were three orders of magnitude higher than compressive moduli (Figs 4c,d versus 3a,b). Interestingly, we showed ultimate tensile strains of all scaffolds to be higher by ~20% in the warp direction than in the weft direction (Fig. 4b, $p < 0.05$).

An important consideration in the interpretation of the current study is that we only used one type of biomaterial (polyglycolic acid yarn), in combination with two different 3D woven structures (with differing degrees of fibre reinforcement) and two different hydrogels (agarose and fibrin). These initial designs represent proof of concept that cartilage-mimicking scaffolds can be constructed with highly controlled mechanical properties by virtue of the 3D fibre reinforcement of the composite structure. However for other applications, any combination of woven fibres and hydrogels with a wide range of physical and mechanical properties may be explored using this 3D weaving technique.

METHODS

Creep experiments were carried out in a confined-compression configuration[2], using an ELF 3200 series precision-controlled materials-testing system (Bose, Minnetonka, Minnesota). Sample thickness was measured optically using a digital video camera (model XDC-X700, Sony Electronics, Park Ridge, New Jersey). Specimens were placed in a confining chamber in a PBS bath and compressive loads were applied using a rigid porous platen. Following equilibration of a 4 gf tare load, a step compressive load of 10 gf was applied to the sample and allowed to equilibrate for 600 s. The compressive modulus (H_A) and an apparent hydraulic permeability (k) were determined using a two-parameter, nonlinear least-squares regression procedure[26,35]. For unconfined compression, strains of $\varepsilon = 0.04$, 0.08, 0.12 and 0.16 were applied to the specimens in a PBS bath after equilibration of a 2% tare strain. Strain steps were held constant for 900 s, allowing the scaffolds to relax to an equilibrium level. Young's modulus was determined by carrying out linear regression on the resulting equilibrium stress–strain plot.

Tensile tests were carried out as described previously for cartilage[35,36] using a materials testing system (SmartTest Series, Bose, Minnetonka, Minnesota). Scaffolds were cut into dumbbell-shaped test specimens (25 mm length). After equilibration of a 10 N tare load for 300 s, samples were tested to failure at a rate of 0.04 mm s^{-1}. Samples were kept wet throughout the test by periodic spraying with PBS. The resulting force (F) was recorded by the load cell and digital data acquisition system and divided by the cross-sectional area (A) for calculation of the tensile stress ($\sigma = F/A$). The ultimate tensile strength, ultimate tensile strain, tensile modulus, energy to failure and Poisson's ratio of the constructs were determined in two (x- or warp and y- or weft) directions. Local strain was determined optically using a digital video system. The tangent modulus was calculated both for the toe (E_0: $\varepsilon = 0$) and in the linear region (E: $\varepsilon = 0.1$) of the resulting stress–strain curve.

Dynamic and stress relaxation shear tests of the composite constructs were carried out in PBS at room temperature using an ARES rheometric system (Rheometric Scientific, Piscataway, New Jersey). First, a series of shear stress relaxation tests were carried out, as described previously[21,37,38]. Three magnitudes of shear strain ($\gamma = 0.001$, 0.0014 and 0.0018) were applied to the sample, followed by a 600 s stress relaxation period. Also, a dynamic frequency sweep was carried out by prescribing a sinusoidal shear strain profile, $\gamma = \gamma_0 \sin(\omega t)$ at γ_0 of 0.05 and ω from 1 to 100 rad s^{-1}.

Two-factor analysis of variance (ANOVA) tests were carried out to compare the different scaffold parameters (pore size and gel type) for compressive and shear biomechanical tests. Statistical significance for tensile testing, which introduced direction (warp and weft) as a third parameter, was assessed using three-factor ANOVA. Statistical significance was reported at the 95% confidence level ($p < 0.05$) for all tests.

Received 3 July 2006; accepted 13 December 2006; published 21 January 2007.

References

1. Mow, V. C., Ratcliffe, A. & Poole, A. R. Cartilage and diarthrodial joints as paradigms for hierarchical materials and structures. *Biomaterials* **13**, 67–97 (1992).
2. Mow, V. C., Kuei, S. C., Lai, W. M. & Armstrong, C. G. Biphasic creep and stress relaxation of articular cartilage in compression? Theory and experiments. *J. Biomech. Eng.* **102**, 73–84 (1980).
3. Soltz, M. A. & Ateshian, G. A. A conewise linear elasticity mixture model for the analysis of tension-compression nonlinearity in articular cartilage. *J. Biomech. Eng.* **122**, 576–586 (2000).
4. Woo, S. L. *et al.* Large deformation nonhomogeneous and directional properties of articular cartilage in uniaxial tension. *J. Biomech.* **12**, 437–446 (1979).
5. Guilak, F., Butler, D. L. & Goldstein, S. A. Functional tissue engineering: the role of biomechanics in articular cartilage repair. *Clin. Orthop. Relat. Res.* S295–S305 (2001).
6. Freed, L. E. *et al.* Biodegradable polymer scaffolds for tissue engineering. *Nature Biotechnol.* **12**, 689–693 (1994).
7. Buschmann, M. D., Gluzband, Y. A., Grodzinsky, A. J., Kimura, J. H. & Hunziker, E. B. Chondrocytes in agarose culture synthesize a mechanically functional extracellular matrix. *J. Orthop. Res.* **10**, 745–758 (1992).
8. Ameer, G. A., Mahmood, T. A. & Langer, R. A biodegradable composite scaffold for cell transplantation. *J. Orthop. Res.* **20**, 16–19 (2002).
9. Freed, L. E., Langer, R., Martin, I., Pellis, N. R. & Vunjak-Novakovic, G. Tissue engineering of cartilage in space. *Proc. Natl Acad. Sci. USA* **94**, 13885–13890 (1997).
10. Gao, J., Dennis, J. E., Solchaga, L. A., Goldberg, V. M. & Caplan, A. I. Repair of osteochondral defect with tissue-engineered two-phase composite material of injectable calcium phosphate and hyaluronan sponge. *Tissue Eng.* **8**, 827–837 (2002).
11. Pei, M. *et al.* Bioreactors mediate the effectiveness of tissue engineering scaffolds. *Faseb J.* **16**, 1691–1694 (2002).
12. Vunjak-Novakovic, G. *et al.* Bioreactor cultivation conditions modulate the composition and mechanical properties of tissue-engineered cartilage. *J. Orthop. Res.* **17**, 130–138 (1999).
13. Tognana, E. *et al.* Adjacent tissues (cartilage, bone) affect the functional integration of engineered calf cartilage in vitro. *Osteoarthritis Cartilage* **13**, 129–138 (2005).
14. Atala, A. *et al.* Injectable alginate seeded with chondrocytes as a potential treatment for vesicoureteral reflux. *J. Urol.* **150**, 745–747 (1993).
15. Caterson, E. J. *et al.* Polymer/alginate amalgam for cartilage-tissue engineering. *Ann. NY Acad. Sci.* **961**, 134–138 (2002).
16. Mauck, R. L. *et al.* Functional tissue engineering of articular cartilage through dynamic loading of chondrocyte-seeded agarose gels. *J. Biomech. Eng.* **122**, 252–260 (2000).
17. Paige, K. T. *et al.* De novo cartilage generation using calcium alginate-chondrocyte constructs. *Plast. Reconstruct. Surgery* **97**, 168–180 (1996).
18. Rowley, J. A., Madlambayan, G. & Mooney, D. J. Alginate hydrogels as synthetic extracellular matrix materials. *Biomaterials* **20**, 45–53 (1999).
19. Marijnissen, W. J. *et al.* Alginate as a chondrocyte-delivery substance in combination with a non-woven scaffold for cartilage tissue engineering. *Biomaterials* **23**, 1511–1517 (2002).
20. Hollister, S. J. Porous scaffold design for tissue engineering. *Nature Mater.* **4**, 518–524 (2005).
21. LeRoux, M. A., Guilak, F. & Setton, L. A. Compressive and shear properties of alginate gel: effects of sodium ions and alginate concentration. *J. Biomed. Mater. Res.* **47**, 46–53 (1999).
22. Mohamed, M. H., Bogdanovich, A. E., Dickinson, L. C., Singletary, J. N. & Lienhart, R. B. A new generation of 3D woven fabric preforms and composites. *Sampe. J.* **37**, 8–17 (2001).
23. Aufderheide, A. C. & Athanasiou, K. A. Comparison of scaffolds and culture conditions for tissue engineering of the knee meniscus. *Tissue Eng.* **11**, 1095–1104 (2005).
24. Benya, P. D. & Shaffer, J. D. Dedifferentiated chondrocytes reexpress the differentiated collagen phenotype when cultured in agarose gels. *Cell* **30**, 215–224 (1982).
25. Lee, D. A. & Bader, D. L. Compressive strains at physiological frequencies influence the metabolism of chondrocytes seeded in agarose. *J. Orthop. Res.* **15**, 181–188 (1997).
26. Cohen, B., Lai, W. M. & Mow, V. C. A transversely isotropic biphasic model for unconfined compression of growth plate and chondroepiphysis. *J. Biomech. Eng.* **120**, 491–496 (1998).
27. Huang, C. Y., Stankiewicz, A., Ateshian, G. A. & Mow, V. C. Anisotropy, inhomogeneity, and tension-compression nonlinearity of human glenohumeral cartilage in finite deformation. *J. Biomech.* **38**, 799–809 (2005).
28. Ateshian, G. A. A theoretical formulation for boundary friction in articular cartilage. *J. Biomech. Eng.* **119**, 81–86 (1997).
29. Soltz, M. A. & Ateshian, G. A. Experimental verification and theoretical prediction of cartilage interstitial fluid pressurization at an impermeable contact interface in confined compression. *J. Biomech.* **31**, 927–934 (1998).
30. Li, W. J., Jiang, Y. J. & Tuan, R. S. Chondrocyte phenotype in engineered fibrous matrix is regulated by fiber size. *Tissue Eng.* **12**, 1775–1785 (2006).
31. Gu, W. Y., Yao, H., Huang, C. Y. & Cheung, H. S. New insight into deformation-dependent hydraulic permeability of gels and cartilage, and dynamic behavior of agarose gels in confined compression. *J. Biomech.* **36**, 593–598 (2003).
32. Akizuki, S. *et al.* Tensile properties of human knee joint cartilage: I. Influence of ionic conditions, weight bearing, and fibrillation on the tensile modulus. *J. Orthop. Res.* **4**, 379–392 (1986).
33. Kempson, G. E., Tuke, M. A., Dingle, J. T., Barrett, A. J. & Horsfield, P. H. The effects of proteolytic enzymes on the mechanical properties of adult human articular cartilage. *Biochim. Biophys. Acta* **428**, 741–760 (1976).
34. Below, S., Arnoczky, S. P., Dodds, J., Kooima, C. & Walter, N. The split-line pattern of the distal femur: A consideration in the orientation of autologous cartilage grafts. *Arthroscopy* **18**, 613–617 (2002).
35. Elliott, D. M., Guilak, F., Vail, T. P., Wang, J. Y. & Setton, L. A. Tensile properties of articular cartilage are altered by meniscectomy in a canine model of osteoarthritis. *J. Orthop. Res.* **17**, 503–508 (1999).

36. Guilak, F., Ratcliffe, A., Lane, N., Rosenwasser, M. P. & Mow, V. C. Mechanical and biochemical changes in the superficial zone of articular cartilage in canine experimental osteoarthritis. *J. Orthop. Res.* **12**, 474–484 (1994).
37. LeRoux, M. A. *et al*. Simultaneous changes in the mechanical properties, quantitative collagen organization, and proteoglycan concentration of articular cartilage following canine meniscectomy. *J. Orthop. Res.* **18**, 383–392 (2000).
38. Zhu, W., Mow, V. C., Koob, T. J. & Eyre, D. R. Viscoelastic shear properties of articular cartilage and the effects of glycosidase treatments. *J. Orthop. Res.* **11**, 771–781 (1993).
39. Bader, D. L., Kempson, G. E., Barrett, A. J. & Webb, W. The effects of leucocyte elastase on the mechanical properties of adult human articular cartilage in tension. *Biochim. Biophys. Acta* **677**, 103–108 (1981).
40. Setton, L. A., Mow, V. C., Muller, F. J., Pita, J. C. & Howell, D. S. Mechanical properties of canine articular cartilage are significantly altered following transection of the anterior cruciate ligament. *J. Orthop. Res.* **12**, 451–463 (1994).
41. Elliott, D. M., Narmoneva, D. A. & Setton, L. A. Direct measurement of the Poisson's ratio of human patella cartilage in tension. *J. Biomech. Eng.* **124**, 223–228 (2002).
42. Huang, C. Y., Mow, V. C. & Ateshian, G. A. The role of flow-independent viscoelasticity in the biphasic tensile and compressive responses of articular cartilage. *J. Biomech. Eng.* **123**, 410–417 (2001).
43. Huang, C. Y., Soltz, M. A., Kopacz, M., Mow, V. C. & Ateshian, G. A. Experimental verification of the roles of intrinsic matrix viscoelasticity and tension-compression nonlinearity in the biphasic response of cartilage. *J. Biomech. Eng.* **125**, 84–93 (2003).
44. Mow, V. C. & Guo, X. E. Mechano-electrochemical properties of articular cartilage: their inhomogeneities and anisotropies. *Annu. Rev. Biomed. Eng.* **4**, 175–209 (2002).
45. Athanasiou, K. A., Rosenwasser, M. P., Buckwalter, J. A., Malinin, T. I. & Mow, V. C. Interspecies comparisons of in situ intrinsic mechanical properties of distal femoral cartilage. *J. Orthop. Res.* **9**, 330–340 (1991).
46. Setton, L. A., Zhu, W. & Mow, V. C. The biphasic poroviscoelastic behavior of articular cartilage: role of the surface zone in governing the compressive behavior. *J. Biomech.* **26**, 581–592 (1993).
47. Athanasiou, K. A., Agarwal, A. & Dzida, F. J. Comparative study of the intrinsic mechanical properties of the human acetabular and femoral head cartilage. *J. Orthop. Res.* **12**, 340–349 (1994).
48. Jurvelin, J. S., Buschmann, M. D. & Hunziker, E. B. Optical and mechanical determination of Poisson's ratio of adult bovine humeral articular cartilage. *J. Biomech.* **30**, 235–241 (1997).
49. Setton, L. A., Mow, V. C. & Howell, D. S. Mechanical behavior of articular cartilage in shear is altered by transection of the anterior cruciate ligament. *J. Orthop. Res.* **13**, 473–482 (1995).

Acknowledgements

Supported by NIH grants AR49294, AR50245, AG15768 and AR48182, NASA grant NNJ04HC72G and a Translational Research Partnership from the Wallace H. Coulter Foundation. The authors thank J. Perera and R. Catz for technical assistance, B. Tawil of Baxter Biosurgery for providing the Tisseel Y used in this study, L. Eibest for assistance with scanning electron microscopy and L. Setton for advice on the mechanical testing.
Correspondence and requests for materials should be addressed to F.G.

Competing financial interests

The authors declare that they have no competing financial interests.

ARTIFICIAL CARTILAGE

Weaving in three dimensions

Despite great expectations, artificial cartilage constructs still represent a challenge for tissue engineers. A three-dimensional fibre–hydrogel material provides a breathrough in the design of scaffolds with mechanical properties that match those of native cartilage.

Gerard A. Ateshian
is in the Departments of Mechanical Engineering and Biomedical Engineering, Columbia University, 500 West 120th St, 220 S.W. Mudd, MC4703, New York, New York 10027, USA.
e-mail: ateshian@columbia.edu

Artificial cartilage has been hailed as the next likely breakthrough in tissue engineering, following manmade skin, and ahead of liver, heart or kidney tissue[1]. With its low cellularity and avascular matrix, cartilage has been considered a good candidate for tissue engineering because of the lesser demand for metabolite transport and the potentially lower risk of implant rejection by the immune system. However, those precious few cartilage cells need to be surrounded by a scaffold that is adequately stiff, otherwise they would be crushed before being able to produce their own new matrix. A fibre–hydrogel composite scaffold presented by Franklin Moutos and colleagues on page 162 of this issue, exhibits mechanical properties that mimic those of healthy cartilage[2], and promise to improve the chances of success of cartilage implants.

The main function of articular cartilage is to serve as a bearing material for movable joints such as the hip, knee or shoulder. It is a connective tissue, millimetres thick, which lines the articulating ends of bones, and exhibits remarkable load-bearing and lubrication properties unmatched by artificial bearings. The main constituents of cartilage are water (75%), collagen (20%) and proteoglycans (5%). The collagen fibrils help the tissue sustain tensile loads while the proteoglycans, which are large negatively charged macromolecules, help it resist compression.

The friction coefficient of articular cartilage can be as low as 0.005, which implies that the frictional force acting tangential to the articular surface may be 200 times smaller than the load transmitted across the joint[3]. There used to be a popular analogy between oil-lubricated bearings of car engines and the viscous synovial fluid that covers the articular surfaces. However, experiments have shown that cartilage can lubricate almost equally well after the synovial fluid has been wiped away[3]. Thus, it is cartilage itself that is primarily responsible for reducing the friction coefficient.

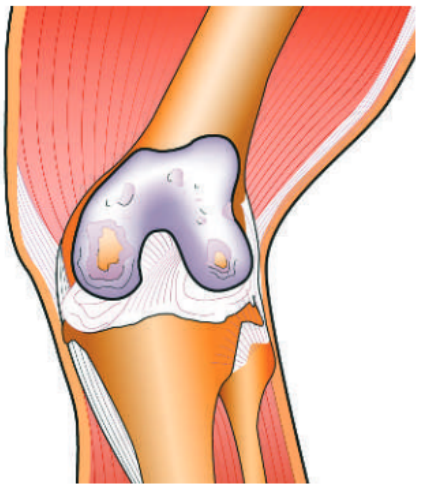

Figure 1 Worn-out cartilage (purple). Osteoarthritis is a painful degenerative disease of articular joints. Full-thickness lesions of the cartilage, resulting from wear and tear, expose the underlying bone, where pain originates in the nerve endings. The high incidence rate of this condition calls for the development of artificial cartilage grafts.

The loads transmitted across lower-extremity joints such as the knee and hip typically range from two to five times body weight. This counter-intuitive observation can be explained by the combination of gravitational forces and the action of muscles that span across a joint and help to stabilize it. Owing to the closeness of muscles to the centre of rotation of a joint, the forces they exert typically far exceed the external loads sustained by the body. These large joint loads are transferred across contacting articular layers, producing contact stresses as high as 12 megapascals. To appreciate the magnitude of this stress, imagine that if you were hanging from a ledge by a fingertip, the pressure on your fingertip would be one megapascal only.

A major challenge of cartilage functional tissue engineering is to produce constructs that are able to sustain these remarkable contact pressures, while also producing low friction coefficients. Fledgling tissue constructs or cell-seeded scaffolds that do not exhibit the properties of native cartilage are likely to be crushed following implantation, unless they are able to acquire these biomechanical properties rapidly, over a reasonable post-operative recovery period. Unfortunately, although chondrocytes (that is, cartilage cells) can synthesize proteoglycans fairly quickly, reaching native levels within a few weeks, collagen synthesis lags very far behind.

The inability to rapidly produce native levels of collagen in engineered cartilage tissue constructs has been particularly troublesome because of the critical biomechanical function of this matrix constituent. It may seem curious at first that the elevated tensile stiffness of cartilage is an important functional property, considering that cartilage layers sustain joint loads in compression only. However, we now understand that the large tensile stiffness of collagen helps cartilage to resist lateral expansion on axial compression; this resistance to volume changes upon loading has the effect of pressurizing the interstitial water of cartilage, considerably increasing its compressive stiffness. This increased stiffness imparted by interstitial fluid pressurization is critical for preventing the crushing of cartilage cells under the very large contact stresses sustained by articular joints. Furthermore, this pressurization turns out to be the primary reason that cartilage exhibits a very low friction coefficient[4]. Indeed, if most of the applied load is supported by pressurized

interstitial fluid, the effective load experienced by the contacting collagen matrices is much reduced and the friction between them is eased.

In this context, the paper by Moutos and co-workers provides a breakthrough in the design of scaffolds whose initial mechanical properties match those of native articular cartilage[2]. These authors have developed a microscale three-dimensional weaving technique to produce scaffolds from yarns made of a biocompatible material such as polyglycolic acid. The fibres in this scaffold are oriented in three orthogonal directions, so as to produce a material with different properties along each of its planes of symmetry. The resulting scaffolds are porous, and the authors filled them with a cell-seeded hydrogel such as agarose or fibrin in which the round morphology and cellular functions typical of chondrocytes can be maintained. Most remarkably, these constructs not only mimic the fibre-composite structure of the native cartilage but they also reproduce the disparity observed between the tensile and compressive stiffness of the tissue, which are critical to load bearing and lubrication. Because the initial mechanical properties of these scaffolds are quite similar to those of native cartilage, it is likely that these constructs will survive the harsh loading environment of the joints immediately after implantation.

This approach represents a paradigm shift in the field of cartilage tissue engineering, which heretofore had proposed that constructs would slowly acquire normal mechanical properties following implantation. The availability of biocompatible, slowly degrading constructs whose initial mechanical properties can be tuned over a broad range (owing to the versatile manufacturing technique) that encompasses those of native cartilage makes it possible to test the hypothesis that initial construct stiffness is critical to the long-term survival of implanted artificial cartilage. The basic premise of this approach is that chondrocytes need to be shielded from excessive compressive strains over a sufficiently long period of time, typically exceeding normal post-operative recovery periods, while they slowly synthesize the collagen matrix critical for their normal function. So the scaffold made by Moutos and co-workers represents a major advance towards this goal, providing an exciting opportunity for cartilage tissue engineers.

References

1. Rawe, J. *Time* **155,** 72–73 (2000).
2. Moutos, F. T., Freed, L. E. & Guilak, F. *Nature Mater.* **6,** 162–167 (2007).
3. Charnley, J. *Ann. Rheum. Dis.* **19,** 10–19 (1960).
4. Krishnan, R., Kopacz, M. & Ateshian, G. A. *J. Orthop. Res.* **22,** 565–570 (2004).

PHASE-CHANGE MATERIALS

Designing optical media of the future

Over the past two decades, the optical recording industry has empirically improved the properties of phase-change materials for rewritable discs. Now a first step has been taken to use computational design to improve these materials.

Friso Jedema
is at NXP Semiconductors, Eindhoven 5656 AA, The Netherlands.
e-mail: friso.jedema@nxp.com

Chalcogenide phase-change materials are the key components used for rewritable optical discs, and improving the speed of imprinting information is of significant commercial interest. Much effort is therefore being expended in the development of these materials, but prediction of the various relevant and desired properties to increase possible writing speeds is difficult, as they are intimately related to the structural changes at the atomic scale. On page 122 of this issue, Matthias Wuttig *et al.*[1] take a big step towards the ability to design novel phase-change materials. By using *ab initio* density functional theory and an improved understanding of the mechanisms behind the structural phase change[2,3], the authors are able to predict the stability of the crystalline state. This could provide valuable information for determining the suitability of chalcogenide materials (for example, Ge–Sb–Te) not only for future optical recording media but also for phase-change random access memories[4] (PCRAM).

Optical writing and erasing bits on a disc is done by heating small spots of a phase-change layer with a focused laser beam, as shown in Fig. 1. Writing involves first the melting of the phase-change material at around 600 °C, followed by a very short cooling time of a few nanoseconds. This enables the material to solidify into an amorphous state, which constitutes the physical representation of a written bit. As the crystalline and amorphous state of the phase-change material have different optical properties, the difference between a crystalline or amorphous spot (or bit) can be read by measuring its reflectance. For erasing a written bit, the same spot of the phase-change layer is heated to only a few hundred degrees Celsius, but now for a duration of tens of nanoseconds. This enables the amorphous material to return into the crystalline state.

Since the first observation of reversible laser-induced amorphous–crystalline transitions by Ovshinsky *et al.*[5], the optical recording industry has been pushing to shorten the bit erasure time, because it is the limiting factor for achieving larger recording speeds. Nowadays a commercial DVD recorder can write a DVD eight times faster than its normal playback speed, corresponding to bit rates as high as 100 Mbit s^{-1} and erasure times of a few tens of nanoseconds. Two classes of phase-change materials were discovered that could deliver these short erasure times, enabled by their fast crystallization speeds[6]: nucleation dominated materials[7] (NDM), first introduced by Matsushita/Panasonic and fast-growth materials[8] (FGM), first introduced by Ricoh. The NDM family has $Ge_2Sb_2Te_5$ (GST 225), $Ge_1Sb_2Te_4$ and $Ge_1Sb_4Te_7$, as its thermodynamic stable ternary compositions[9], all residing along the pseudobinary $GeTe–Sb_2Te_3$ tie-line, as